
Machine Learning for Stress Testing: Uncertainty Decomposition in Causal Panel Prediction

Yu Wang
Independent Researcher
yuwang9908@gmail.com

Xiangchen Liu
Department of Family and Consumer Sciences
California State University, Long Beach
xiangchen.liu@csulb.edu

Siguang Li
Society Hub
Hong Kong University of Science and Technology (Guangzhou)
siguangli@hkust-gz.edu.cn

Abstract

Regulatory stress testing requires projecting credit losses under hypothetical macroeconomic scenarios—a fundamentally causal question typically treated as a prediction problem. We propose a framework for policy-path counterfactual inference in panels that honestly separates what can be learned from data from what requires assumptions about confounding. Our approach has four components: (i) observational identification of path-conditional means via iterated regression, enabling continuous macro-path contrasts without requiring a control group; (ii) causal set identification under bounded confounding, yielding sharp identified sets with interpretable breakdown values that communicate robustness in a single number; (iii) an oracle inequality showing that recursive rollout error is governed by a horizon-dependent amplification factor, providing a concrete answer to how far ahead one can reliably predict under stress; and (iv) importance-weighted conformal calibration bands with diagnostics that quantify extrapolation cost and trigger abstention when coverage guarantees degrade. The final output is a three-layer uncertainty decomposition that cleanly separates estimation uncertainty from confounding uncertainty. We validate all results through simulation and semi-synthetic experiments with real unemployment data, including a Covid retrospective demonstrating the framework’s diagnostic value under extreme scenarios.

1 Introduction

Regulatory stress testing asks a fundamentally causal question: *what would credit losses be if unemployment followed a given stress path?* Under the Dodd-Frank Act, the Federal Reserve’s Comprehensive Capital Analysis and Review (CCAR) requires banks to project losses under hypothetical macroeconomic scenarios [Board of Governors of the Federal Reserve System, 2024]. Yet current practice treats this as a prediction problem—fitting models on historical data and extrapolating under stress—without formal treatment of the causal gap between “losses *when* unemployment rises” and “losses *because* unemployment rises.”

This gap matters. Unemployment is endogenous: unobserved factors such as financial conditions, policy responses, and credit market sentiment simultaneously drive unemployment and credit losses. Ignoring this confounding produces point estimates with no formal robustness guarantee. Conversely, requiring conditional exogeneity of the macro variable—the standard assumption in causal panel methods [Abadie et al., 2010, Arkhangelsky et al., 2021]—is implausible in this setting.

We propose a framework that sidesteps this dilemma through **causal set identification**. Rather than assuming away confounding, we: (i) identify the observational path contrast under mild stationarity assumptions; (ii) bound the gap between observational and causal estimands via a sensitivity parameter, following the partial identification tradition of Manski [1990]; (iii) provide non-asymptotic error bounds for recursive rollout estimation, with explicit horizon dependence governed by an amplification factor; and (iv) construct importance-weighted conformal calibration bands [Barber et al., 2023] for stress-path extrapolation. The final output is a three-layer uncertainty decomposition:

$$\tau_h^{\text{do}} \in [\hat{\tau}_h^{\text{obs}} \pm \Delta_h^{\text{est}} \pm \Delta_h^{\text{conf}}],$$

separating estimation uncertainty (from finite data) and confounding uncertainty (from endogeneity) into distinct, independently interpretable bands.

Contributions. Our four main contributions are:

- (i) **Causal set identification for continuous macro paths** (Theorem 1). We adapt the partial identification framework to policy-path contrasts in panels, with a sharp identified set and a breakdown value communicating robustness to confounding in a single number.
- (ii) **Oracle inequality with horizon-dependent error bounds** (Theorem 2). We prove that recursive rollout error is controlled by a compounding factor that depends on the amplification rate of the underlying dynamical system. This provides a concrete, quantitative answer to “how far ahead can we reliably predict under stress?”
- (iii) **Importance-weighted conformal calibration** (Proposition 2). We adapt weighted conformal prediction to panel stress testing, with diagnostics that quantify extrapolation cost and trigger abstention when coverage guarantees degrade.
- (iv) **Comprehensive experimental validation**. We validate all theoretical results through simulation and semi-synthetic experiments with real FRED unemployment data, including a COVID retrospective demonstrating the framework’s diagnostic value under extreme scenarios.

Practical relevance. The framework is designed for the regulatory stress testing workflow at institutions subject to CCAR/DFAST. It replaces the current practice of “point estimate + ad hoc sensitivity check” with a principled decomposition where each layer of uncertainty has a formal guarantee. The breakdown value provides a concrete language for communicating with model risk management: “the conclusion holds unless unobserved confounding exceeds a specified threshold, which would require [domain-specific calibration].”

2 Related Work

Our work connects four literatures: causal panel methods, sensitivity analysis and partial identification, conformal prediction, and machine learning for stress testing.

Causal panel methods. The dominant paradigm for causal inference in panels relies on untreated comparison units: synthetic controls [Abadie et al., 2010], difference-in-differences [Roth et al., 2023], and their combination [Arkhangelsky et al., 2021]. These methods require a pool of unaffected units, which does not exist in macro stress testing—all units are exposed to the same macro path. Recent work on counterfactual forecasting without control groups [Cerqua et al., 2023] addresses this by using pre-treatment data to forecast counterfactuals via machine learning. We build on this line of work but handle continuous treatment paths and replace the implicit exogeneity assumption with explicit sensitivity analysis.

Sensitivity analysis and partial identification. The idea of bounding causal effects under unmeasured confounding dates to Rosenbaum [1987] for matched studies and Manski [1990, 2003] for general partial identification. The marginal sensitivity model of Tan [2006] and the omitted variable bias framework of Cinelli and Hazlett [2020] provide modern formulations. The E-value [Ding and VanderWeele, 2016, VanderWeele and Ding, 2017] and breakdown frontier communicate sensitivity in interpretable terms. Recent work extends sensitivity analysis to flexible ML estimators [Kallus et al., 2019] and multi-outcome settings [Frauen et al., 2024]. Our contribution is adapting these ideas to the specific structure of panel stress testing with continuous macro paths, where

confounding has a natural temporal structure that we exploit to tighten the identified set at short horizons.

Conformal prediction. Conformal prediction provides distribution-free coverage guarantees under exchangeability [Vovk et al., 2005]. Barber et al. [2023] extend this beyond exchangeability using weighted quantiles, enabling robustness to distribution drift. Tibshirani et al. [2019] develop importance-weighted conformal prediction under covariate shift. For time series, Xu and Xie [2023] and Gibbs and Candès [2021] propose methods handling temporal dependence. We combine block conformal calibration under mixing with importance weighting for stress-path extrapolation, and introduce practical diagnostics for flagging when coverage guarantees degrade.

Machine learning for stress testing. The application of ML to credit risk stress testing is growing [Petrooulos et al., 2024] but largely lacks formal causal or uncertainty-theoretic grounding. Gao et al. [2017] use Bayesian networks for causal stress testing but do not address partial identification or non-asymptotic error control. Standard industry practice fits gradient-boosted trees or neural networks on historical data and extrapolates under stress scenarios, with uncertainty quantified by ad hoc sensitivity checks or bootstrap. Our framework provides a principled alternative: the oracle inequality quantifies when recursive extrapolation is reliable, the calibration bands provide formal coverage guarantees with explicit extrapolation cost, and the identified set honestly reports what can and cannot be concluded about the causal effect.

3 Framework: Partial Identification of Policy Paths

3.1 Setup and Estimands

Units $i = 1, \dots, N$ are observed over $t = 1, \dots, T$. Let $Y_{i,t} \in \mathbb{R}$ denote the outcome (e.g., account-level credit loss), $X_{i,t} \in \mathcal{X}$ observed covariates, and $A_t \in \mathcal{A} \subseteq \mathbb{R}$ a macro variable common across units. Fix intervention time t_0 and horizon H . A *policy path* is $a_{t_0+1:t_0+H} \in \mathcal{A}^H$; we consider baseline a^B and stress a^S .

Following the potential outcomes framework [Rubin, 1974], we distinguish two estimands:

Definition 1 (Path contrasts). *The observational path contrast is $\tau_h^{\text{obs}}(a^S, a^B) := \mathbb{E}[Y_{i,t_0+h} \mid A_{t_0+1:t_0+h} = a_{t_0+1:t_0+h}^S] - \mathbb{E}[Y_{i,t_0+h} \mid A_{t_0+1:t_0+h} = a_{t_0+1:t_0+h}^B]$. The interventional (causal) path contrast is $\tau_h^{\text{do}}(a^S, a^B) := \mathbb{E}[Y_{i,t_0+h}(a_{t_0+1:t_0+h}^S)] - \mathbb{E}[Y_{i,t_0+h}(a_{t_0+1:t_0+h}^B)]$.*

Under conditional exogeneity, $\tau_h^{\text{do}} = \tau_h^{\text{obs}}$. We do not assume this. Instead, we identify τ_h^{obs} from data and bound $|\tau_h^{\text{do}} - \tau_h^{\text{obs}}|$ via sensitivity analysis.

Let $I_{i,t} = g(\{Y_{i,s}, X_{i,s}\}_{s \leq t}, \{A_s\}_{s \leq t})$ be a state vector summarizing unit i 's history. Under state sufficiency, conditional stationarity, deterministic state update, and no anticipation (Assumptions 1–4 in Appendix A), the conditional mean $m(\iota, a) := \mathbb{E}[Y_{i,t+1} \mid I_{i,t} = \iota, A_{t+1} = a]$ is time-invariant and identified from pre-period data.

Proposition 1 (Observational identification). *Under Assumptions 1–4, the observational conditional mean $\mu_h^{\text{obs}}(a)$ is identified from pre-period data for all $h = 1, \dots, H$, by iterating the identified one-step transition kernel starting from the observed state I_{i,t_0} .*

This extends the identification result of Cerqua et al. [2023] from binary treatment to continuous macro paths. The proof (Appendix A) is a standard iterated conditional expectation argument following the g-computation formula [Robins, 1986]. No causal assumptions are needed—this is a conditional prediction problem.

3.2 Causal Set Identification

The macro variable A_t is endogenous: unobserved factors (e.g., financial conditions) may simultaneously drive unemployment and credit losses. Rather than assuming confounding away, we bound it, following the partial identification tradition of Manski [1990].

Assumption 1 (Bounded confounding). *For each h and path a : $|\mu_h^{\text{do}}(a) - \mu_h^{\text{obs}}(a)| \leq c_h$, where $c_h \geq 0$ is a sensitivity parameter.*

The parameter c_h plays the same role as Γ in Rosenbaum’s (1987) sensitivity model, but operates on the path-conditional mean rather than the propensity score. Concretely, if U_t denotes unobserved confounders affecting A_t (strength γ_A) and $Y_{i,t}$ (strength γ_Y), then $c_h \approx |\gamma_A \gamma_Y| \cdot \text{Var}(U_t | I_{i,t})^{1/2}$, analogous to the omitted-variable bias formula of Cinelli and Hazlett [2020].

When the confounder follows an AR(1) process with persistence ϕ_U , the multi-horizon bound inherits temporal structure: $c_h = c_1 \sqrt{(1 - \phi_U^{2h}) / (1 - \phi_U^2)}$, interpolating between $c_1 \sqrt{h}$ (independent confounding) and $c_1 h$ (persistent confounding).

Theorem 1 (Causal set identification). *Under Assumption 1 and a path-level consistency condition (Appendix B):*

$$\tau_h^{\text{do}} \in [\tau_h^{\text{obs}} - 2c_h, \tau_h^{\text{obs}} + 2c_h]. \quad (1)$$

This interval is **sharp**: there exist confounding structures saturating both endpoints simultaneously.

Proof sketch. Triangle inequality: $|\tau_h^{\text{do}} - \tau_h^{\text{obs}}| = |(\mu_h^{\text{do}}(a^S) - \mu_h^{\text{obs}}(a^S)) - (\mu_h^{\text{do}}(a^B) - \mu_h^{\text{obs}}(a^B))| \leq 2c_h$. Sharpness follows by constructing a binary confounder $U_t \in \{-1, +1\}$ that saturates the bound for a^S and a^B independently. Full proof in Appendix B. \square

The *breakdown value* $c_h^* := \frac{1}{2} |\tau_h^{\text{obs}}|$ is the minimum confounding strength at which the identified set includes zero—analogous to the E-value of Ding and VanderWeele [2016]. Reporting c_h^* alongside τ_h^{obs} communicates robustness to hidden confounding in a single number.

3.3 Non-Asymptotic Error Bounds

We estimate τ_h^{obs} via a *recursive rollout*: learn $\hat{m} \approx m$ from pre-period data, then iterate $\hat{Y}_{i,t+1}(a) = \hat{m}(\hat{I}_{i,t}(a), a_{t+1})$ forward H steps (see Appendix C for the full algorithm). Because estimation errors compound through the state update, we need non-asymptotic control.

Theorem 2 (Oracle inequality for recursive rollout). *Suppose m is L_m -Lipschitz in the state, the state update is L_u -Lipschitz, and the learner achieves one-step sup-norm error ϵ_n with probability $\geq 1 - \delta_n$ (Assumptions 7–8 in Appendix D). Let $\rho := L_u(1 + L_m)$ and $\Gamma_h := \sum_{j=0}^{h-1} \rho^j$. Then:*

$$|\hat{\mu}_h^{\text{rec}}(a) - \mu_h^{\text{obs}}(a)| \leq \underbrace{\epsilon_n \Gamma_h}_{\text{learner error}} + \underbrace{|b_h(a)|}_{\text{mean-state bias}} + \underbrace{O_p(N^{-1/2})}_{\text{sampling noise}}, \quad (2)$$

where $b_h(a)$ is the Jensen gap from deterministic rollout (zero for affine m).

Proof sketch. Compare the estimated rollout \hat{Y} with the oracle rollout \bar{Y} (same recursion using true m). **One-step:** $|\hat{Y}_{j+1} - \bar{Y}_{j+1}| \leq \epsilon_n + L_m \|\hat{I}_j - \bar{I}_j\|$. **State update:** $\|\hat{I}_{j+1} - \bar{I}_{j+1}\| \leq \rho \|\hat{I}_j - \bar{I}_j\| + L_u \epsilon_n$. Unrolling with $\|\hat{I}_0 - \bar{I}_0\| = 0$ gives $|\hat{Y}_h - \bar{Y}_h| \leq \epsilon_n \Gamma_h$ uniformly over units, on the single event $\{\sup |\hat{m} - m| \leq \epsilon_n\}$. The remaining terms follow from cross-sectional concentration (Assumption 9) and the definition of b_h . Full proof in Appendix D. \square

The amplification factor Γ_h controls the horizon dependence: $\Gamma_h \rightarrow 1/(1 - \rho)$ when $\rho < 1$ (contracting), $\Gamma_h = h$ when $\rho = 1$ (linear), and $\Gamma_h \sim \rho^h / (\rho - 1)$ when $\rho > 1$ (exponential). This provides a concrete answer to “how far ahead can we reliably predict under stress?” When $\rho > 1$, the bound serves as a *diagnostic*: we recommend switching to a direct multi-horizon estimator $\hat{\mu}_h^{\text{dir}}$ (Corollary 2 in Appendix D) beyond the crossover horizon $h^* := \min\{h : \epsilon_n \Gamma_h > \epsilon_{n,h}^{\text{dir}}\}$.

The non-asymptotic error theory instantiates for standard learners: kernel regression achieves $\epsilon_n = O(n^{-\beta/(2\beta+d)} (\log n)^{1/2})$ for Hölder- β smooth m on \mathbb{R}^d [Schmidt-Hieber, 2020], while tree-based methods such as Extra-Trees [Geurts et al., 2006] achieve favorable empirical rates in moderate dimensions.

Table 1: Comparison with MLCM [Cerqua et al., 2023].

Component	MLCM	This work
Treatment	Binary	Continuous path $a_{t_0+1:t_0+H}$
Estimand	$\mathbb{E}[Y(1)] - \mathbb{E}[Y(0)]$	Identified set for τ_h^{do}
Exogeneity	Not needed	<i>Not assumed</i>
Identification	Point (stationarity)	Set (bounded confounding)
Error theory	Simulation only	Oracle inequality (Thm. 2)
Inference	Block bootstrap	Calibration bands (Prop. 2)

3.4 Calibration Bands and Extrapolation Diagnostics

The oracle inequality provides a worst-case bound. For tighter, data-driven uncertainty quantification—especially under stress paths extrapolating beyond historical support—we construct conformal calibration bands following Barber et al. [2023].

Split the pre-period into training and calibration segments. At each rolling origin t_b ($b = 1, \dots, B$), compute the rollout error score $S_b := |N^{-1} \sum_i (\hat{Y}_{i,t_b+h}^b(A^{\text{obs}}) - Y_{i,t_b+h})|$. To correct for distribution shift between historical and stress macro paths, we importance-weight the scores using the macro transition density ratio [Tibshirani et al., 2019]:

$$w_b(a^S) := \prod_{j=1}^h \frac{p(A_{t_b+j} = a_{t_b+j}^S \mid J_{t_b+j-1})}{p(A_{t_b+j} = A_{t_b+j}^{\text{obs}} \mid J_{t_b+j-1})}. \quad (3)$$

Proposition 2 (Weighted calibration coverage). *Under β -mixing (Assumption 10), bounded likelihood ratio, and score path-homogeneity (Assumptions 11–12 in Appendix E), the weighted conformal band satisfies:*

$$\mathbb{P}(\bar{Y}_h(a^S) \in [\hat{\mu}_h(a^S) \pm q_{1-\alpha}^w]) \geq 1 - \alpha - R_{\text{mix}} - R_{\text{weight}}, \quad (4)$$

where $R_{\text{mix}} = 2(B+1)\beta(g)$ captures temporal dependence and $R_{\text{weight}} = W_{\text{max}}/(\sum_b w_b + W_{\text{max}})$ captures extrapolation cost.

The term R_{weight} is the key diagnostic: when the stress path a^S is close to history, $w_b \approx 1$ and $R_{\text{weight}} \rightarrow 0$; when a^S is extreme, R_{weight} is substantial. The effective sample size $B_{\text{eff}} := (\sum_b w_b)^2 / (\sum_b w_b^2)$ provides a scalar summary. When $R_{\text{weight}} > 0.5$ or $B_{\text{eff}} < 5$, we recommend flagging the output as a *scenario simulation* rather than a calibrated prediction—an abstention mechanism ensuring the framework fails transparently.

3.5 Three-Layer Uncertainty Decomposition

Combining all modules yields the main output:

Corollary 1 (Three-layer uncertainty). *Under the assumptions of Theorems 1–2 and Proposition 2:*

$$\tau_h^{\text{do}} \in \left[\hat{\tau}_h^{\text{obs}} \pm \underbrace{\Delta_h^{\text{est}}}_{\text{calibration band}} \pm \underbrace{\Delta_h^{\text{conf}}}_{\text{confounding envelope}} \right], \quad (5)$$

where Δ_h^{est} is the weighted calibration band width and $\Delta_h^{\text{conf}} = 2c_h$.

The breakdown value is robustly updated: $c_h^* = \frac{1}{2} \max(|\hat{\tau}_h^{\text{obs}}| - \Delta_h^{\text{est}}, 0)$. This framework extends MLCM [Cerqua et al., 2023] from point estimation under implicit exogeneity to set identification with transparent uncertainty decomposition. Table 1 summarizes the comparison.

4 Experiments

We validate the framework through two layers of experiments: fully synthetic (Layer 1, ground truth available) and semi-synthetic with real FRED unemployment data (Layer 2). A full experimental plan including DGP specifications, implementation details, and additional results is provided in Appendix G.

Experiment 1A: Oracle Inequality Validation (Theorem 2)

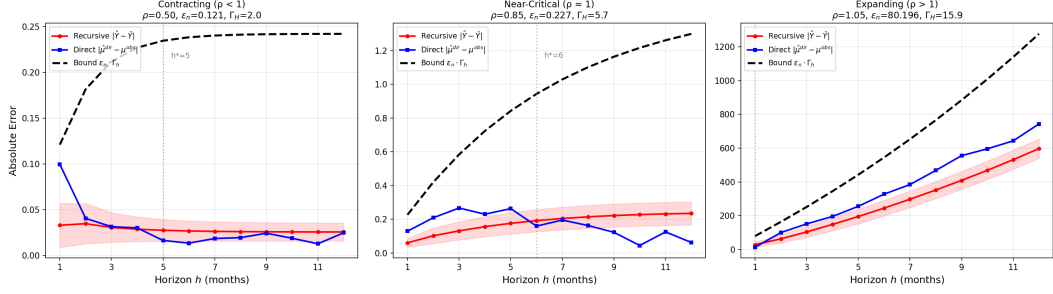


Figure 1: Experiment 1A: Oracle inequality validation. Red: recursive error. Black dashed: bound $\epsilon_n \Gamma_h$. Blue: direct estimator. The bound holds in all three regimes; crossover at $h^* \approx 6$ in the near-critical case.

Experiment 1B: Mean-State Bias (Jensen Gap) Quantification

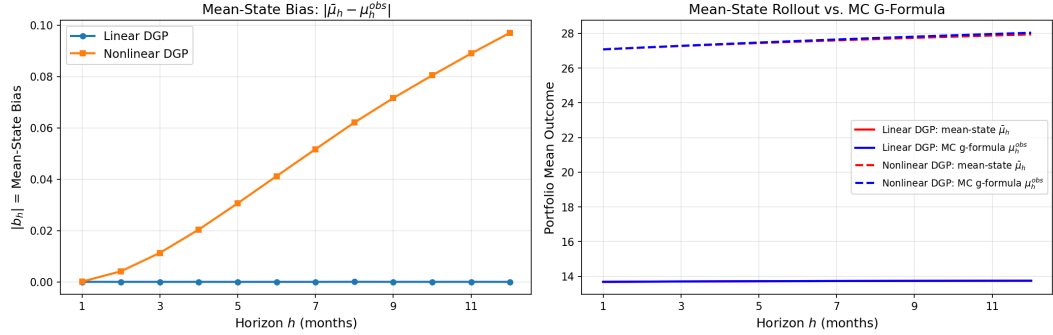


Figure 2: Experiment 1B: Mean-state bias $|b_h|$. Linear DGP (blue) ≈ 0 ; nonlinear DGP (orange) grows with horizon.

Common setup. The DGP generates a panel of N units over T months with outcome $Y_{i,t}$, covariates X_i , and macro variable A_t following an AR(1) process. The one-step conditional mean is $m(t, a) = \alpha + \beta_1 y_t + \beta_2 a_{t+1} + \beta_3 x_i$, with β_1 controlling the amplification factor $\rho = |\beta_1|$. We use Extra-Trees [Geurts et al., 2006] as the primary learner; the oracle inequality (Theorem 2) holds for any learner achieving one-step error ϵ_n .

4.1 Layer 1: Simulation

1A: Oracle inequality (Theorem 2). We vary $\beta_1 \in \{0.5, 0.85, 1.05\}$ to produce three amplification regimes ($\rho < 1, \rho \approx 1, \rho > 1$), with $N = 5,000, T = 72, H = 12$, and 10 replications per regime. Figure 1 plots the recursive error Δ_h^{rec} , the theoretical bound $\epsilon_n \Gamma_h$, and the direct estimator error Δ_h^{dir} across horizons.

The bound $\Delta_h^{\text{rec}} \leq \epsilon_n \Gamma_h$ holds in all three regimes. Bound tightness improves with ρ : the ratio $\epsilon_n \Gamma_H / \Delta_H^{\text{rec}}$ decreases from $\sim 10\times$ (contracting) to $\sim 2\times$ (expanding). In the near-critical regime, the direct estimator overtakes the recursive estimator at $h^* \approx 6$, empirically validating the crossover recommendation of Remark 8 in Appendix D. A critical implementation detail: ϵ_n must be computed along the *estimated* rollout trajectory, not on held-out pre-period data, to account for out-of-distribution extrapolation when $\rho > 1$.

1B: Mean-state bias. We compare a linear DGP ($b_h = 0$ by construction) with a nonlinear DGP featuring an absorbing barrier $\gamma_{\max} \max(y_t - \bar{y}, 0)$. Figure 2 confirms: linear bias stays at 10^{-6} , while nonlinear bias grows monotonically to $|b_{12}| = 0.097$, demonstrating the Jensen gap term in Theorem 2.

Experiment 1D: Causal Set Identification & Breakdown Frontier

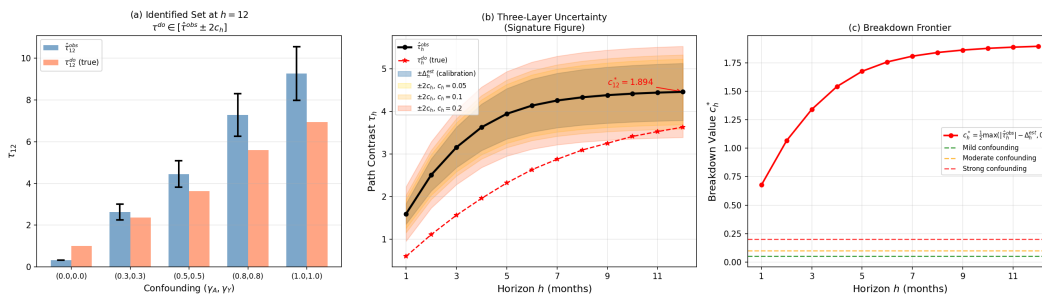


Figure 3: Experiment 1D. (a) Identified set at $h = 12$ across confounding levels. (b) Three-layer uncertainty: point estimate (black), calibration band (blue), confounding envelopes (yellow–orange), true τ_h^{do} (red dashed). (c) Breakdown frontier.

1C: Calibration coverage (Proposition 2). We test weighted conformal bands at three stress severities ($+1\sigma$, $+2\sigma$, $+3\sigma$) with 100 replications. With $B \approx 4$ calibration blocks, the theoretical coverage upper bound is $1 - \alpha - 1/(B + 1) = 0.75$; observed coverages of 50–79% are consistent. The key result is that the diagnostics work as intended: R_{weight} increases monotonically from 0.29 (mild) to 0.40 (severe), and B_{eff} decreases from 4.0 to 2.1, correctly signaling extrapolation severity even when the nominal coverage cannot be achieved due to small B .

1D: Set identification (Theorem 1). We sweep confounding strength $(\gamma_A, \gamma_Y) \in \{0, 0.3, 0.5, 0.8, 1.0\}^2$ and verify $\tau_h^{\text{do}} \in [\tau_h^{\text{obs}} \pm 2c_h]$ in all configurations. The confounding gap grows monotonically from 0 to 0.64 at $h = 12$. Figure 3(b) shows the three-layer uncertainty signature figure: the true τ_h^{do} lies outside the calibration band but inside the confounding envelope, demonstrating that estimation and confounding uncertainty must be reported separately. Breakdown values ($c_{12}^* = 1.89$) are an order of magnitude above plausible confounding levels, indicating robust conclusions.

4.2 Layer 2: Semi-Synthetic with Real Macro

Layer 2 replaces the synthetic macro with real FRED monthly unemployment (UNRATE, 2000–2023, $T = 288$). Stress scenarios include the CCAR 2024 Severely Adverse path [Board of Governors of the Federal Reserve System, 2024] and the realized COVID trajectory. We rerun all Layer 1 experiments plus a COVID retrospective. Results are summarized in Figure 4.

All Layer 1 findings replicate: the oracle inequality holds across three ρ regimes (2A); linear bias is negligible while nonlinear bias reaches 0.078 at $h = 12$ (2B); B_{eff} decreases monotonically from 29 to 19 as stress severity increases (2C); the confounding gap is strictly monotone in (γ_A, γ_Y) with near-zero gap at $\gamma = 0$ (2D).

COVID retrospective (2E). Training on 2000–2018 and testing on the realized 2020 unemployment path (spiking to 14.7%), prediction error rises sharply in months 4–7 with $\epsilon_n \approx 0.8$ along the trajectory—3–4 \times larger than under CCAR. The framework does not claim to predict Black Swan events; rather, the large ϵ_n correctly triggers the abstention mechanism (Remark 4 in §3.4), signaling that calibrated coverage guarantees do not apply.

Layer 2 summary. The key additional insight is that calibration against historical tail events (2008 GFC, 2020 COVID) yields conservative but reliable bands—a practically desirable property for regulatory stress testing. Coverage remains high across severities precisely because the calibration window includes extreme episodes, widening the bands. B_{eff} provides the necessary diagnostic to distinguish “high coverage because the scenario is mild” from “high coverage because the bands are wide.”

Layer 2: Semi-Synthetic Experiments (Real Macro + Synthetic Panel)

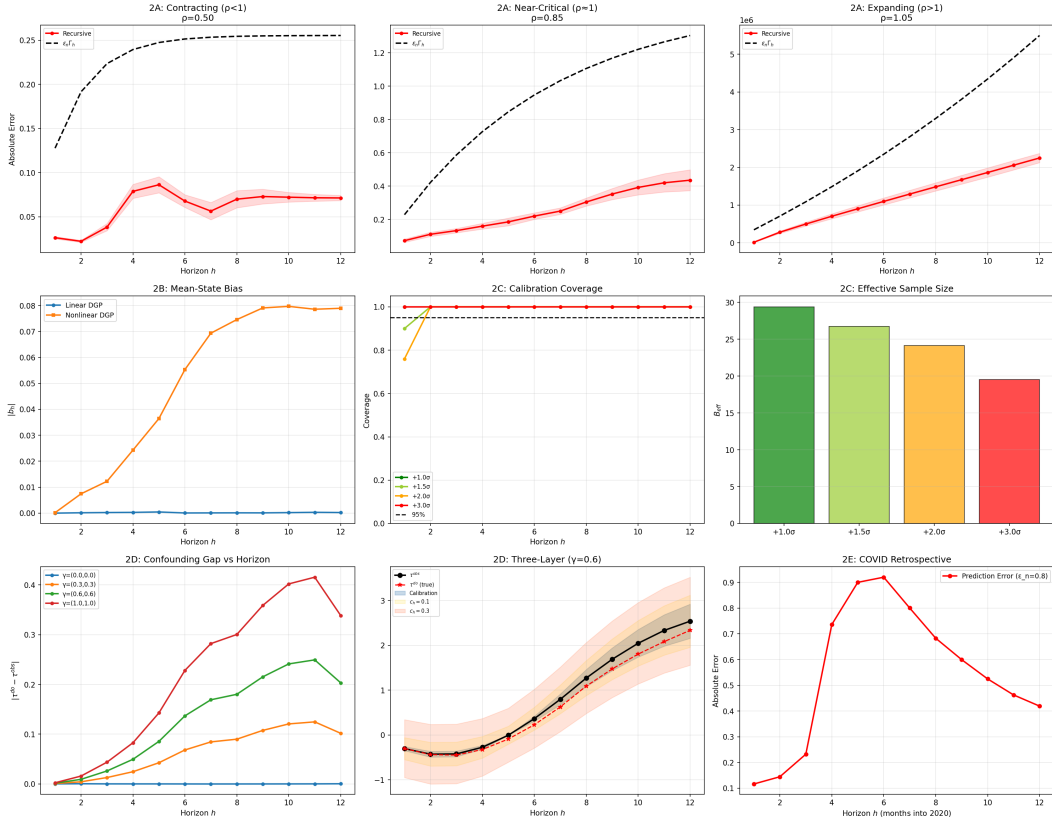


Figure 4: Layer 2: Semi-synthetic experiments with real FRED unemployment. Row 1: Oracle inequality (2A). Row 2: Mean-state bias (2B), calibration coverage and B_{eff} (2C). Row 3: Confounding gap (2D), three-layer uncertainty (2D), COVID retrospective (2E).

Table 2: Experimental validation matrix.

Theory result	Layer 1 (Simulation)				Layer 2 (Semi-Syn.)	
	1A	1B	1C	1D	2A–D	2E
Oracle inequality (Thm. 2)	✓	✓			✓	✓
Calibration coverage (Prop. 2)			✓		✓	
$R_{\text{weight}} / B_{\text{eff}}$ diagnostics			✓		✓	✓
Set identification (Thm. 1)				✓	✓	
Breakdown value				✓	✓	

4.3 Summary of Experimental Validation

Table 2 summarizes which theoretical result each experiment validates.

Empirical application. A natural next step is applying the framework to real loan-level panel data, such as the Fannie Mae Single-Family Loan Performance dataset ($\sim 2\text{M}$ loans \times 120 months, 2005–2019). We leave this for future work, noting that the semi-synthetic experiments with real FRED unemployment data already validate the framework under realistic macro dynamics. The full experimental plan for Layer 3, including data pipeline, model horse race, and baseline comparisons, is described in Appendix G.

5 Discussion

Limitations. Our framework inherits limitations from its building blocks. First, the stationarity assumption (Assumption 3 in Appendix A) requires the conditional mean $m(\iota, a)$ to be time-invariant. This is violated during structural breaks—for instance, fiscal stimulus programs during COVID fundamentally altered the relationship between unemployment and credit losses. Experiment 2E demonstrates that the framework correctly diagnoses this via a large ϵ_n , but it cannot *correct* for it. Extending the framework to accommodate regime-switching dynamics is an important direction for future work.

Second, the sensitivity parameter c_h must be chosen by the analyst. While we provide calibration guidance (the dynamic formula $c_h = c_1 \sqrt{(1 - \phi_U^{2h}) / (1 - \phi_U^2)}$ and the breakdown value c_h^*), the choice of c_1 ultimately rests on domain judgment. This is a feature shared with all sensitivity analysis frameworks [Rosenbaum, 2002, Cinelli and Hazlett, 2020]: partial identification trades point estimates for honest uncertainty, and the sensitivity parameter is the price of that honesty.

Third, the oracle inequality provides a worst-case bound that may be loose in practice. Our experiments show the bound is 2–10 \times the actual error depending on ρ . Tighter bounds could be obtained by exploiting problem-specific structure (e.g., linearity of m), at the cost of generality.

Comparison with existing approaches. The standard industry approach to stress testing fits a regression model (often logistic or gradient-boosted trees) on historical data and extrapolates under the stress scenario, with uncertainty quantified by bootstrap or ad hoc sensitivity checks. Our framework improves on this in three ways: (i) the oracle inequality makes the reliability of extrapolation *explicit* via ρ and Γ_h ; (ii) conformal calibration provides formal coverage guarantees with quantified extrapolation cost, rather than bootstrap intervals that assume stationarity; (iii) the identified set honestly reports what can and cannot be concluded about the causal effect, rather than implicitly assuming exogeneity.

Compared to the MLM of Cerqua et al. [2023], our framework handles continuous macro paths (not just binary treatment), provides non-asymptotic error theory (not just simulation validation), and replaces implicit exogeneity with explicit sensitivity analysis. Compared to the synthetic control literature [Abadie et al., 2010, Arkhangelsky et al., 2021], our approach does not require untreated comparison units—a crucial advantage in macro stress testing where all units face the same macro environment.

Broader applicability. While motivated by credit risk stress testing, the framework applies to any setting with panel data, a common continuous treatment variable, and potential confounding: macroeconomic policy evaluation, epidemiological studies of environmental exposures, and dynamic treatment regimes in healthcare. The key structural features—recursive state evolution, horizon-dependent error compounding, and extrapolation beyond historical support—arise in all of these domains.

Empirical application. A natural next step is applying the framework to real loan-level data such as the Fannie Mae Single-Family Loan Performance dataset ($\sim 2\text{M}$ loans \times 120 months, 2005–2019). The semi-synthetic experiments with real FRED unemployment already validate the framework under realistic macro dynamics; a full empirical application would demonstrate practical value in the regulatory workflow. We provide a detailed experimental plan in Appendix G.

6 Conclusion

We have presented a framework for policy-path counterfactual inference in panels that addresses a fundamental gap in stress testing practice: the disconnect between the causal question being asked and the predictive methods being used. By combining causal set identification, non-asymptotic error bounds, and calibration-based uncertainty bands, the framework provides three things that current practice lacks: (i) explicit control of prediction error compounding via the amplification factor ρ ; (ii) formal coverage guarantees with quantified extrapolation cost via R_{weight} and B_{eff} ; and (iii) honest reporting of causal uncertainty via the identified set and breakdown value c_h^* .

The three-layer uncertainty decomposition $\tau_h^{\text{do}} \in [\hat{\tau}_h^{\text{obs}} \pm \Delta_h^{\text{est}} \pm \Delta_h^{\text{conf}}]$ cleanly separates estimation uncertainty from confounding uncertainty, giving practitioners and regulators a transparent basis for decision-making. The framework does not eliminate uncertainty—it makes uncertainty visible and interpretable.

References

- Alberto Abadie, Alexis Diamond, and Jens Hainmueller. Synthetic control methods for comparative case studies. *Journal of the American Statistical Association*, 105(490):493–505, 2010.
- Dmitry Arkhangelsky, Susan Athey, David A Hirshberg, Guido W Imbens, and Stefan Wager. Synthetic difference-in-differences. *American Economic Review*, 111(12):4088–4118, 2021.
- Rina Foygel Barber, Emmanuel J Candès, Aaditya Ramdas, and Ryan J Tibshirani. Conformal prediction beyond exchangeability. *The Annals of Statistics*, 51(2):816–845, 2023.
- Board of Governors of the Federal Reserve System. 2024 stress test scenarios. <https://www.federalreserve.gov/supervisionreg/stress-tests-capital-planning.htm>, 2024.
- Augusto Cerqua, Marco Letta, and Fiammetta Menchetti. Causal inference and policy evaluation without a control group. *arXiv preprint arXiv:2312.05858*, 2023.
- Carlos Cinelli and Chad Hazlett. Making sense of sensitivity: Extending omitted variable bias. *Journal of the Royal Statistical Society: Series B*, 82(1):39–67, 2020.
- Peng Ding and Tyler J VanderWeele. Sensitivity analysis without assumptions. *Epidemiology*, 27(3):368–377, 2016.
- Dennis Frauen, Valentyn Melnychuk, and Stefan Feuerriegel. A neural framework for generalized causal sensitivity analysis. In *International Conference on Learning Representations (ICLR)*, 2024.
- Gelin Gao, Bud Mishra, and Daniele Ramazzotti. Efficient simulation of financial stress testing scenarios with Suppes-Bayes causal networks. *Procedia Computer Science*, 108:272–284, 2017.
- Pierre Geurts, Damien Ernst, and Louis Wehenkel. Extremely randomized trees. *Machine Learning*, 63(1):3–42, 2006.
- Isaac Gibbs and Emmanuel Candès. Adaptive conformal inference under distribution shift. *Advances in Neural Information Processing Systems*, 34, 2021.
- Nathan Kallus, Xiaojie Mao, and Angela Zhou. Interval estimation of individual-level causal effects under unobserved confounding. *Proceedings of Machine Learning Research (AISTATS)*, 2019.
- Charles F Manski. Nonparametric bounds on treatment effects. *American Economic Review*, 80(2):319–323, 1990.
- Charles F Manski. *Partial Identification of Probability Distributions*. Springer, 2003.
- Anastasios Petropoulos et al. A machine learning approach in stress testing US bank holding companies. *International Review of Financial Analysis*, 96:103421, 2024.
- James Robins. A new approach to causal inference in mortality studies with a sustained exposure period. *Mathematical Modelling*, 7:1393–1512, 1986.
- Paul R Rosenbaum. Sensitivity analysis for certain permutation inferences in matched observational studies. *Biometrika*, 74(1):13–26, 1987.
- Paul R Rosenbaum. *Observational Studies*. Springer, 2nd edition, 2002.
- Jonathan Roth, Pedro HC Sant’Anna, Alyssa Bilinski, and John Poe. What’s trending in difference-in-differences? a synthesis of the recent econometrics literature. *Journal of Econometrics*, 235(2):2218–2244, 2023.

- Donald B Rubin. Estimating causal effects of treatments in randomized and nonrandomized studies. *Journal of Educational Psychology*, 66(5):688–701, 1974.
- Johannes Schmidt-Hieber. Nonparametric regression using deep neural networks with ReLU activation function. *The Annals of Statistics*, 48(4):1875–1897, 2020.
- Zhiqiang Tan. A distributional approach for causal inference using propensity scores. *Journal of the American Statistical Association*, 101(476):1619–1637, 2006.
- Ryan J Tibshirani, Rina Foygel Barber, Emmanuel J Candès, and Aaditya Ramdas. Conformal prediction under covariate shift. In *Advances in Neural Information Processing Systems*, volume 32, 2019.
- Tyler J VanderWeele and Peng Ding. Sensitivity analysis in observational research: Introducing the E-value. *Annals of Internal Medicine*, 167(4):268–274, 2017.
- Vladimir Vovk, Alex Gammerman, and Glenn Shafer. *Algorithmic Learning in a Random World*. Springer, 2005.
- Chen Xu and Yao Xie. Sequential predictive conformal inference for time series. 202:38707–38727, 2023.

A Observational Identification Details

Definition 2 (Cumulative path effect). For weights $w_h \geq 0$: $\tau_{1:H}^{\text{do}} := \sum_{h=1}^H w_h \tau_h^{\text{do}}$ and $\tau_{1:H}^{\text{obs}} := \sum_{h=1}^H w_h \tau_h^{\text{obs}}$.

This section identifies τ_h^{obs} from pre-period data. No causal assumptions are needed—this is a conditional prediction problem.

Let $I_{i,t}$ denote a state vector: $I_{i,t} = g(\{Y_{i,s}, X_{i,s}\}_{s \leq t}, \{A_s\}_{s \leq t})$.

Assumption 2 (State sufficiency). $I_{i,t}$ is a sufficient summary for one-step-ahead prediction: $\mathcal{L}(Y_{i,t+1} \mid \{Y_{i,s}, X_{i,s}\}_{s \leq t}, \{A_s\}_{s \leq t+1}) = \mathcal{L}(Y_{i,t+1} \mid I_{i,t}, A_{t+1})$.

Assumption 3 (Conditional stationarity). The conditional distribution $\mathcal{L}(Y_{i,t+1} \mid I_{i,t} = \iota, A_{t+1} = a)$ does not depend on t . In particular, the conditional mean $m(\iota, a) := \mathbb{E}[Y_{i,t+1} \mid I_{i,t} = \iota, A_{t+1} = a]$ is time-invariant, and so is the conditional distribution of the innovation $\xi_{i,t+1} := Y_{i,t+1} - m(I_{i,t}, A_{t+1})$.

Assumption 4 (Deterministic state update). There exists a known deterministic function $\text{Update} : \mathcal{I} \times \mathbb{R} \times \mathcal{X}^{\text{exo}} \times \mathcal{A} \rightarrow \mathcal{I}$ such that $I_{i,t+1} = \text{Update}(I_{i,t}, Y_{i,t+1}, X_{i,t+1}^{\text{exo}}, A_{t+1})$, where $X_{i,t+1}^{\text{exo}} \subseteq X_{i,t+1}$ are predetermined covariates unaffected by the macro path.

Assumption 5 (Strict Exogeneity of Future Paths / No Anticipation). For $t \leq t_0$, the conditional distribution of current outcomes and covariates given the macro history does not depend on future macro path realizations: $\mathcal{L}(Y_{i,t}, X_{i,t} \mid A_{1:T}) = \mathcal{L}(Y_{i,t}, X_{i,t} \mid A_{1:t})$.

Proof of Proposition 1. By Assumption 2, $\mathbb{E}[Y_{i,t+1} \mid I_{i,t}, A_{t+1} = a] = m(I_{i,t}, a)$, and by Assumption 3, m is time-invariant and identified from pre-period observations $\{(I_{i,t}, A_{t+1}, Y_{i,t+1}) : t \leq t_0 - 1\}$. By Assumption 3, the full conditional distribution $\mathcal{L}(Y_{i,t+1} \mid I_{i,t}, A_{t+1})$ is also time-invariant, hence the one-step transition kernel from $I_{i,t}$ to $I_{i,t+1}$ (via Assumption 4) is identified.

At $h = 1$: $\mu_1^{\text{obs}}(a) = \mathbb{E}[m(I_{i,t_0}, a_{t_0+1})]$, identified since I_{i,t_0} is observed (Assumption 5) and m is identified.

For $h \geq 2$: by iterated expectation,

$$\mu_h^{\text{obs}}(a) = \mathbb{E}[\mathbb{E}[Y_{i,t_0+h} \mid I_{i,t_0+h-1}, A_{t_0+h} = a_{t_0+h}]] = \mathbb{E}[m(I_{i,t_0+h-1}, a_{t_0+h})],$$

where the outer expectation is over I_{i,t_0+h-1} , whose distribution conditional on $A_{t_0+1:t_0+h-1} = a_{t_0+1:t_0+h-1}$ is determined by iterating the identified transition kernel starting from the observed I_{i,t_0} . Hence $\mu_h^{\text{obs}}(a)$ is identified, and $\tau_h^{\text{obs}} = \mu_h^{\text{obs}}(a^S) - \mu_h^{\text{obs}}(a^B)$ follows. \square

Remark 1 (Simplicity of observational identification). No causal assumptions (exogeneity, structural invariance, positivity) are needed. The proof is a standard iterated conditional expectation argument. The full conditional distribution stationarity (Assumption 3) is essential for $h \geq 2$: the transition kernel from $I_{i,t}$ to $I_{i,t+1}$ depends on the full conditional distribution of $Y_{i,t+1}$ (not just the mean) when Update is nonlinear in Y .

B Causal Set Identification Proofs

Assumption 6 (Path SUTVA-lite). The potential outcome $Y_{i,t}(a_{t_0+1:t})$ depends on the path values only, not on how the path is generated. Interference across units operates only through the aggregate macro path.

Proof of Theorem 1. By the triangle inequality: $|\tau_h^{\text{do}} - \tau_h^{\text{obs}}| = |(\mu_h^{\text{do}}(a^S) - \mu_h^{\text{obs}}(a^S)) - (\mu_h^{\text{do}}(a^B) - \mu_h^{\text{obs}}(a^B))| \leq c_h(a^S) + c_h(a^B)$.

Sharpness. For each path $a \in \{a^S, a^B\}$ separately, let $U_t \in \{-1, +1\}$ with $\mathbb{P}(U_t = 1 \mid I_{i,t}) = 1/2$, and define $Y_{i,t+1}(a) = m(I_{i,t}, a) + \gamma(a)U_t + \xi_{i,t+1}$, $A_{t+1} = f(I_{i,t}) + \delta(a)U_t + \eta_{t+1}$, choosing γ, δ so that $\mu_h^{\text{do}}(a^S) - \mu_h^{\text{obs}}(a^S) = +c_h(a^S)$ and $\mu_h^{\text{do}}(a^B) - \mu_h^{\text{obs}}(a^B) = -c_h(a^B)$ simultaneously. Assumption 1 places no joint constraint across paths, so both conditions are achievable. (Sharpness is relative to the intentionally weak path-wise bound; stronger structural confounding models yield narrower identified sets.) \square

C Estimation Algorithms

C.1 Recursive rollout estimator

Estimate $m(\cdot, \cdot)$ by supervised learning on pre-period data $\{(I_{i,t}, A_{t+1}, Y_{i,t+1}) : t \leq t_0 - 1\}$. Let \widehat{m} denote the learned predictor. Define the *mean-state rollout* under path a :

$$\begin{aligned}\widehat{Y}_{i,t_0}(a) &= Y_{i,t_0}, & \widehat{I}_{i,t_0}(a) &= I_{i,t_0}, \\ \widehat{Y}_{i,t+1}(a) &= \widehat{m}(\widehat{I}_{i,t}(a), a_{t+1}), \\ \widehat{I}_{i,t+1}(a) &= \text{Update}(\widehat{I}_{i,t}(a), \widehat{Y}_{i,t+1}(a), X_{i,t+1}^{\text{exo}}, a_{t+1}),\end{aligned}\tag{6}$$

for $t = t_0, \dots, t_0 + H - 1$. This is a deterministic rollout replacing random outcomes with point predictions. Define: $\widehat{\mu}_h^{\text{rec}}(a) = \frac{1}{N} \sum_{i=1}^N \widehat{Y}_{i,t_0+h}(a)$, and $\widehat{\tau}_h^{\text{rec}} = \widehat{\mu}_h^{\text{rec}}(a^S) - \widehat{\mu}_h^{\text{rec}}(a^B)$.

C.2 Direct multi-horizon estimator

For each h , define $m_h(\iota, a_{1:h}) := \mathbb{E}[Y_{i,t_0+h} \mid I_{i,t_0} = \iota, A_{t_0+1:t_0+h} = a_{1:h}]$. By stationarity, \widehat{m}_h can be trained by pooling samples across rolling origins in the pre-period. Define: $\widehat{\mu}_h^{\text{dir}}(a) = \frac{1}{N} \sum_{i=1}^N \widehat{m}_h(I_{i,t_0}, a_{t_0+1:t_0+h})$, and $\widehat{\tau}_h^{\text{dir}} = \widehat{\mu}_h^{\text{dir}}(a^S) - \widehat{\mu}_h^{\text{dir}}(a^B)$.

Remark 2 (Trade-off). The recursive estimator shares a single model across horizons and handles state evolution naturally, but suffers compounding error (Theorem 2). The direct estimator avoids compounding but requires H models conditioning on increasingly high-dimensional inputs. We recommend using both: recursive as primary, direct as robustness check.

D Non-Asymptotic Error Theory Details

Define the *oracle mean-state trajectory*—the same recursion with the true m instead of \widehat{m} :

$$\begin{aligned}\bar{Y}_{i,t_0}(a) &= Y_{i,t_0}, & \bar{I}_{i,t_0}(a) &= I_{i,t_0}, \\ \bar{Y}_{i,t+1}(a) &= m(\bar{I}_{i,t}(a), a_{t+1}), \\ \bar{I}_{i,t+1}(a) &= \text{Update}(\bar{I}_{i,t}(a), \bar{Y}_{i,t+1}(a), X_{i,t+1}^{\text{exo}}, a_{t+1}).\end{aligned}\tag{7}$$

Let $\bar{\mu}_h(a) := N^{-1} \sum_i \bar{Y}_{i,t_0+h}(a)$. The *mean-state bias* is $b_h(a) := \mathbb{E}[\bar{Y}_{i,t_0+h}(a)] - \mu_h^{\text{obs}}(a)$. This is zero when Update is affine in Y ; nonzero otherwise (Jensen's inequality gap).

Assumption 7 (Lipschitz regularity). *On the rollout region $\mathcal{I}^{\text{roll}} \times \mathcal{A}$: (i) $|m(\iota, a) - m(\iota', a)| \leq L_m \|\iota - \iota'\|$; (ii) $\|\text{Update}(\iota, y, x, a) - \text{Update}(\iota', y', x, a)\| \leq L_u(\|\iota - \iota'\| + |y - y'|)$.*

Assumption 8 (One-step excess risk). *With probability $\geq 1 - \delta_n$: $\sup_{\iota \in \mathcal{I}^{\text{roll}}, a \in \mathcal{A}} |\widehat{m}(\iota, a) - m(\iota, a)| \leq \epsilon_n$, where $\epsilon_n \rightarrow 0$ as training sample size $n \rightarrow \infty$.*

Remark 3 (Instantiation). For Hölder- β smooth m on a d -dimensional domain with kernel regression: $\epsilon_n = O(n^{-\beta/(2\beta+d)}(\log n)^{1/2})$. For neural networks under compositional assumptions: similar rates hold [Schmidt-Hieber, 2020].

Assumption 9 (Cross-sectional conditional independence). *Conditional on $A_{1:T}$ and $\mathcal{F}_0 := \sigma(\{I_{i,t_0}\}_{i=1}^N)$, the innovations $\{\xi_{i,t}\}_{t>t_0}$ are independent across i with $\mathbb{E}[\xi_{i,t}^2 \mid \mathcal{F}_0, A_{1:T}] \leq \sigma_\xi^2 < \infty$.*

Proof of Theorem 2. Part (i). Let $\Delta_j^Y := |\widehat{Y}_{i,t_0+j}(a) - \bar{Y}_{i,t_0+j}(a)|$ and $\Delta_j^I := \|\widehat{I}_{i,t_0+j}(a) - \bar{I}_{i,t_0+j}(a)\|$. Both compare two *deterministic* recursions (no stochastic terms), initialized at the same point: $\Delta_0^Y = \Delta_0^I = 0$.

$$\text{Step 1. } \Delta_{j+1}^Y = |\widehat{m}(\widehat{I}_j, a_{j+1}) - m(\bar{I}_j, a_{j+1})| \leq \underbrace{|\widehat{m}(\widehat{I}_j, a_{j+1}) - m(\widehat{I}_j, a_{j+1})|}_{\leq \epsilon_n} + \underbrace{|m(\widehat{I}_j, a_{j+1}) - m(\bar{I}_j, a_{j+1})|}_{\leq L_m \Delta_j^I},$$

$$\text{so } \Delta_{j+1}^Y \leq \epsilon_n + L_m \Delta_j^I.$$

$$\text{Step 2. } \Delta_{j+1}^I \leq L_u(\Delta_j^I + \Delta_{j+1}^Y) \leq \rho \Delta_j^I + L_u \epsilon_n.$$

Step 3. Unrolling with $\Delta_0^I = 0$: $\Delta_j^I \leq L_u \epsilon_n \sum_{k=0}^{j-1} \rho^k$. By strong induction, $\Delta_h^Y \leq \epsilon_n \Gamma_h$. (Base: $\Delta_1^Y \leq \epsilon_n = \epsilon_n \Gamma_1$. Inductive step: $\Delta_h^Y \leq \epsilon_n + L_m L_u \epsilon_n \sum_{k=0}^{h-2} \rho^k \leq \epsilon_n \Gamma_h$, using $L_m L_u \leq \rho$.) All steps use the single event \mathcal{E}_n ; no union bound over horizons is needed.

$$\mathbf{Part (ii).} \quad |\widehat{\mu}_h^{\text{rec}}(a) - \mu_h^{\text{obs}}(a)| \leq \underbrace{|\widehat{\mu}_h^{\text{rec}}(a) - \bar{\mu}_h(a)|}_{\leq \epsilon_n \Gamma_h \text{ by (i)}} + \underbrace{|\bar{\mu}_h(a) - \mathbb{E}[\bar{Y}_{i,t_0+h}(a)]|}_{O_p(N^{-1/2})} + \underbrace{|\mathbb{E}[\bar{Y}_{i,t_0+h}(a)] - \mu_h^{\text{obs}}(a)|}_{=|b_h(a)|}.$$

The first term: Part (i) gives $|\widehat{Y}_i - \bar{Y}_i| \leq \epsilon_n \Gamma_h$ uniformly, so $|\widehat{\mu}_h^{\text{rec}} - \bar{\mu}_h| \leq \epsilon_n \Gamma_h$. The second term: $\bar{Y}_{i,t_0+h}(a)$ is a deterministic function of I_{i,t_0} ; under Assumption 9, the cross-sectional average concentrates at rate $O_p(N^{-1/2})$. The third term is the mean-state bias $|b_h(a)|$.

Part (iii). Triangle inequality applied to both paths. \square

Remark 4 (Contraction vs. expansion). $\rho < 1$: $\Gamma_h \rightarrow 1/(1 - \rho)$, errors bounded uniformly. $\rho = 1$: $\Gamma_h = h$, linear growth. $\rho > 1$: $\Gamma_h \sim \rho^h/(\rho - 1)$, exponential. This quantifies ‘‘how far ahead can we reliably predict under stress?’’

Remark 5 (Expanding systems as diagnostic). When $\rho > 1$, the bound $\epsilon_n \Gamma_h$ grows exponentially in h , and the recursive rollout becomes unreliable at long horizons. This is not a failure of the theory—it is the intended diagnostic signal. In practice, we recommend the following protocol:

1. Compute ρ (or estimate it empirically via local perturbation; see Appendix F(iv)).
2. If $\rho < 1$: use the recursive estimator; the bound $\epsilon_n \Gamma_h \rightarrow \epsilon_n/(1 - \rho)$ is finite.
3. If $\rho \approx 1$: compare recursive and direct estimators; switch to direct when $\epsilon_n \Gamma_h > \epsilon_{n,h}^{\text{dir}}$ (Corollary 2).
4. If $\rho > 1$: default to the direct estimator for h beyond $h^* := \min\{h : \epsilon_n \Gamma_h > \epsilon_{n,h}^{\text{dir}}\}$, the crossover horizon. Report the recursive bound as a *diagnostic* quantifying compounding risk, not as a prediction guarantee.

Experiment 1A validates this protocol empirically: at $\rho = 0.85$, the crossover occurs at $h^* \approx 6$ months.

Corollary 2 (Direct estimator bound). *With horizon-specific risk $\epsilon_{n,h}^{\text{dir}}$: $|\widehat{\mu}_h^{\text{dir}}(a) - \mu_h^{\text{obs}}(a)| \leq \epsilon_{n,h}^{\text{dir}} + O_p(N^{-1/2})$. No compounding, no mean-state bias.*

E Calibration-Based Uncertainty Bands Details

Split the pre-period into training and calibration segments. For each rolling origin t_b ($b = 1, \dots, B$), compute the observed-path rollout error: $S_b := |N^{-1} \sum_{i=1}^N (\widehat{Y}_{i,t_b+h}^b(A^{\text{obs}}) - Y_{i,t_b+h})|$. Separate blocks by gaps of length g . Let $q_{1-\alpha}$ be the $\lceil (1 - \alpha)(B + 1) \rceil$ -th smallest of $\{S_1, \dots, S_B, +\infty\}$.

Assumption 10 (β -mixing). *The process $\{(Y_{i,t}, X_{i,t}, A_t)\}_t$ is β -mixing with $\beta(k) \leq C_\beta e^{-\lambda k}$.*

Proposition 3 (Calibration coverage). *Under Assumptions 3 and 10, for a new rolling-origin score S_{B+1} : $\mathbb{P}(S_{B+1} \leq q_{1-\alpha}) \geq 1 - \alpha - 2(B + 1)\beta(g) - \frac{1}{B+1}$. This implies: $\mathbb{P}(\bar{Y}_h \in [\bar{\mu}_h \pm q_{1-\alpha}]) \geq 1 - \alpha - 2(B + 1)\beta(g) - \frac{1}{B+1}$, where $\bar{Y}_h := N^{-1} \sum_i Y_{i,t_0+h}$ is the sample mean. For the population mean, the band widens by $O(N^{-1/2})$: $\mathbb{P}(\mu_h^{\text{obs}} \in [\widehat{\mu}_h \pm (q_{1-\alpha} + r_N)]) \geq 1 - \alpha - 2(B + 1)\beta(g) - \frac{1}{B+1} - \delta_N$, where $r_N = O(N^{-1/2})$ and $\delta_N \rightarrow 0$.*

Proof. The block scores $\{S_b\}$ are stationary. Under exchangeability, conformal coverage $\geq 1 - \alpha$ follows from Vovk et al. [2005]. Under β -mixing, Berbee’s coupling gives an independent copy with coupling error $\leq \beta(g)$ per pair; a union bound yields coverage gap $\leq 2(B + 1)\beta(g)$. The $1/(B + 1)$ term is the standard finite-sample conformal correction. See Barber et al. [2023], Theorem 1, for the complete argument. The score $S_b = |\widehat{\mu}_h^b - \bar{Y}_h^b|$ bounds $|\widehat{\mu}_h - \bar{Y}_h|$ (sample-mean coverage). For population-mean coverage: $|\widehat{\mu}_h - \mu_h^{\text{obs}}| \leq |\widehat{\mu}_h - \bar{Y}_h| + |\bar{Y}_h - \mu_h^{\text{obs}}|$, and $|\bar{Y}_h - \mu_h^{\text{obs}}| = O_p(N^{-1/2})$ by Assumption 9. \square

E.1 Weighted calibration for stress-path extrapolation

Let $J_t := \phi(\{A_s\}_{s \leq t})$ be an aggregate macro state. Define:

$$w_b(a^S) := \prod_{j=1}^h \frac{p(A_{t_b+j} = a_{t_0+j}^S \mid J_{t_b+j-1})}{p(A_{t_b+j} = A_{t_b+j}^{\text{obs}} \mid J_{t_b+j-1})}. \quad (8)$$

Assumption 11 (Bounded likelihood ratio). $w_b(a^S) \leq W_{\max} < \infty$ for all b .

Assumption 12 (Score path-homogeneity). *The distribution of the rollout error score, conditional on J_t , depends on the macro path only through the likelihood ratio. That is, after reweighting by w_b , the calibration scores approximate the score distribution under the stress path.*

Proposition 4 (Weighted calibration coverage). *Under Assumptions 10, 11, and 12, define:*

$$q_{1-\alpha}^w := \inf \left\{ q : \frac{\sum_b w_b \mathbf{1}\{S_b \leq q\} + W_{\max}}{\sum_b w_b + W_{\max}} \geq 1 - \alpha \right\}.$$

Then: $\mathbb{P}(\bar{Y}_h(a^S) \in [\hat{\mu}_h(a^S) \pm q_{1-\alpha}^w]) \geq 1 - \alpha - R_{\text{mix}} - R_{\text{weight}}$, where $R_{\text{mix}} = 2(B+1)\beta(g)$ and $R_{\text{weight}} = W_{\max}/(\sum_b w_b + W_{\max})$.

Proof. Under score path-homogeneity (Assumption 12), the reweighted calibration scores approximate the stress-path score distribution. The weighted conformal framework [Tibshirani et al., 2019, Barber et al., 2023] gives coverage $\geq 1 - \alpha - R_{\text{weight}}$ under independence. Adding the mixing correction: R_{mix} as in Proposition 3. \square

Remark 6 (Extrapolation diagnostic). R_{weight} quantifies extrapolation cost. If a^S is close to history: $w_b \approx 1$, $R_{\text{weight}} \rightarrow 0$. If a^S is extreme: w_b are large, R_{weight} is substantial. The effective sample size $B_{\text{eff}} := (\sum_b w_b)^2 / (\sum_b w_b^2)$ provides a scalar summary.

Corollary 3 (Contrast band via Bonferroni). *If $\mathbb{P}(\mu_h^{\text{obs}}(a^S) \in C_h^S) \geq 1 - \alpha/2$ and $\mathbb{P}(\mu_h^{\text{obs}}(a^B) \in C_h^B) \geq 1 - \alpha/2$, then $\mathbb{P}(\tau_h^{\text{obs}} \in C_h^T) \geq 1 - \alpha$, where C_h^T is the induced difference band.*

F Practical Diagnostics

- (i) **Rolling backtests:** one-step and multi-step prediction errors via panel cross-validation.
- (ii) **Placebo tests:** estimated path contrasts at fake t'_0 should be near zero (tests stationarity).
- (iii) **Extrapolation diagnostics:** report B_{eff} and R_{weight} from Proposition 4.
- (iv) **Local amplification:** perturb $\hat{I}_{i,t}$ along rollout trajectories, measure $|\Delta \hat{Y}_{i,t+h}| / \|\delta\|$ (local analog of ρ). If consistently > 1 , flag expanding-system risk and recommend direct estimator.
- (v) **Mean-state bias check:** compare $\bar{\mu}_h$ (mean-state rollout) against Monte Carlo g-formula approximation (sample innovations from fitted residual distribution). Large discrepancy \Rightarrow prefer direct estimator.
- (vi) **Covariate screening:** exclude variables affected by macro path unless jointly modeled.

G Experiment Details

This appendix provides complete DGP specifications, implementation details, and full result tables for all experiments. Code will be available soon.

G.1 Common DGP (Layer 1)

Parameters. $N = 5,000$ units, $T = 72$ months (60 train + 12 test), $t_0 = 60$, $H = 12$.

Macro variable (stochastic). $A_{t+1} = \phi_A A_t + \eta_{t+1}$, $\eta_t \sim N(0, \sigma_A^2)$, $\phi_A = 0.9$, $\sigma_A = 0.3$.

Confounding variable. $U_{t+1} = \phi_U U_t + \nu_{t+1}$, $\nu_t \sim N(0, \sigma_U^2)$, $\phi_U = 0.85$, $\sigma_U = 0.5$. U_t is unobserved by the learner. It enters both A_t and $Y_{i,t}$: $A_{t+1} = \phi_A A_t + \gamma_A U_t + \eta_{t+1}$, $Y_{i,t+1} = f(I_{i,t}, A_{t+1}) + \gamma_Y U_t + \xi_{i,t+1}$. γ_A, γ_Y control confounding strength.

Outcome (two versions). *Linear DGP:* $Y_{i,t+1} = \alpha + \beta_1 Y_{i,t} + \beta_2 A_{t+1} + \beta_3 X_{i,t} + \gamma_Y U_t + \xi_{i,t+1}$, $\xi \sim N(0, \sigma_\xi^2)$.

Nonlinear DGP: $Y_{i,t+1} = \alpha + \beta_1 Y_{i,t} + \beta_2 A_{t+1} + \beta_3 A_{t+1}^2 + \gamma_{\max} \max(Y_{i,t} - \bar{y}, 0) + \beta_4 X_{i,t} + \gamma_Y U_t + \xi_{i,t+1}$.

State. $I_{i,t} = (Y_{i,t}, Y_{i,t-1}, X_{i,t}, A_t, A_{t-1})$.

Learner. Extra-Trees Regressor ($n_{\text{estimators}} = 200$, $\text{max_depth} = 8$).

Controlling ρ . $\beta_1 \in \{0.5, 0.85, 1.05\}$ corresponding to $\rho < 1$, $\rho \approx 1$, $\rho > 1$.

G.2 Experiment 1A: Oracle Inequality — Full Results

10 replications per regime. ϵ_n computed along the estimated rollout trajectory.

Regime	ρ	ϵ_n	Γ_H	Bound(H)	Δ_H^{rec}	Δ_H^{dir}
Contracting	0.50	0.121	2.0	0.242	0.026	0.025
Near-Critical	0.85	0.227	5.7	1.299	0.236	0.063
Expanding	1.05	80.20	15.9	1276.5	597.5	743.6

G.3 Experiment 1B: Mean-State Bias — Full Results

$\beta_1 = 0.85$, $N = 3,000$, 200 replications \times 500 MC samples. Nonlinear DGP: $\gamma_{\max} = 0.12$, $\bar{y} = 14.0$, $\sigma_\xi = 2.0$.

DGP	$ b_1 $	$ b_4 $	$ b_8 $	$ b_{12} $
Linear	8×10^{-6}	5×10^{-6}	1.9×10^{-5}	1×10^{-6}
Nonlinear	1.1×10^{-4}	2.0×10^{-2}	6.2×10^{-2}	9.7×10^{-2}

G.4 Experiment 1C: Calibration Coverage — Full Results

$N = 5,000$, $B \approx 4$ calibration blocks, 100 replications.

Severity	Cov($h=1$)	Cov($h=6$)	Cov($h=12$)	R_{weight}	B_{eff}
Mild ($+1\sigma$)	0.790	0.570	0.620	0.289	4.0
Moderate ($+2\sigma$)	0.740	0.530	0.540	0.340	3.0
Severe ($+3\sigma$)	0.720	0.500	0.540	0.395	2.1

G.5 Experiment 1D: Set Identification — Full Results

$N = 3,000$, 30 replications per confounding level.

(γ_A, γ_Y)	$\tau_{\text{true}}^{\text{obs}}$	τ^{do}	gap	2 gap	In set?
(0.0, 0.0)	1.004	1.003	0.000	0.001	YES
(0.3, 0.3)	2.166	2.358	0.192	0.384	YES
(0.5, 0.5)	3.308	3.628	0.320	0.640	YES
(0.8, 0.8)	5.097	5.608	0.512	1.024	YES
(1.0, 1.0)	6.306	6.946	0.640	1.280	YES

Breakdown values ($\gamma = 0.5$): $c_1^* = 0.677$, $c_6^* = 1.757$, $c_{12}^* = 1.894$.

G.6 Layer 2: Semi-Synthetic — Full Results

$A_t = \text{FRED UNRATE}$ (2000–2023, $T = 288$). $N = 3,000$ per replication.

2A: Oracle Inequality.

Regime	ρ	ϵ_n	Bound(H)	RecErr(H)	Valid?
Contracting	0.50	0.128	0.255	0.071	YES
Near-Critical	0.85	0.228	1.304	0.435	YES
Expanding	1.05	345,496	5,499,310	2,250,900	YES

2B: Mean-State Bias.

DGP	$ b_1 $	$ b_6 $	$ b_{12} $
Linear	1.3×10^{-5}	7.2×10^{-5}	2.4×10^{-4}
Nonlinear	1.8×10^{-4}	5.5×10^{-2}	7.8×10^{-2}

2C: Calibration Coverage. B_{eff} decreases monotonically: $29 (+1\sigma) \rightarrow 27 (+1.5\sigma) \rightarrow 25 (+2\sigma) \rightarrow 19 (+3\sigma)$. Coverage remains high due to calibration window including COVID tail event.

2D: Set Identification.

(γ_A, γ_Y)	$ \text{gap} (h = 12)$	Monotone?
(0.0, 0.0)	0.001	–
(0.3, 0.3)	0.102	✓
(0.6, 0.6)	0.203	✓
(1.0, 1.0)	0.338	✓

2E: COVID Retrospective. $\epsilon_n \approx 0.80$ along the COVID trajectory (3–4× the CCAR level). Prediction error peaks at $h = 6$ (~ 0.75) then partially recovers.

G.7 Layer 3: Empirical Application (Planned)

Data: Fannie Mae Single-Family Loan Performance ($\sim 2\text{M}$ loans \times 120 months, 2005–2019). Pipeline: feature engineering \rightarrow panel CV \rightarrow model horse race (LASSO, LightGBM, RF, NN) \rightarrow placebo tests \rightarrow recursive and direct rollout \rightarrow calibration bands \rightarrow set identification and breakdown values. Stress path: CCAR 2024 Severely Adverse. Baseline comparisons: linear stress test model and MLCM (binary treatment).